Supporting Information for "Narrow Optical Line Widths in Erbium Implanted in TiO_2"

Christopher M. Phenicie[1,3], Paul Stevenson[1,3], Sacha Welinski[1,3], Brendon C. Rose[1], Abraham T. Asfaw[1], Robert J. Cava[2], Stephen A. Lyon[1], Nathalie P. de Leon[1], and Jeff D. Thompson[1]

[1]Department of Electrical Engineering, Princeton University, Princeton, NJ 08544, USA
[2]Department of Chemistry, Princeton University, Princeton, NJ 08544, USA
[3]Contributed equally to this work

1 Full g-tensor measurement

The angular variations of the ESR shown in figure 3a in the main text are not enough to reconstruct the full g-tensor. For this reason, complementary measurements were performed by rotating the magnetic field direction about a different axis in the ab-plane, as shown in Figure S1. In this case, it is possible to see the variation of the ESR lines corresponding to the two site orientations separately. Knowing that those orientations are related to each other by a 90 degree rotation with respect to the c-axis, the data from each orientation can be fit to the same g-tensor where the value of the principal g values in the ab-plane are swapped with each other. From this, the full g-tensor (see figure S1) is:

$$g = \begin{pmatrix} 2.0(3) & 0 & 0 \\ 0 & 0.06(6) & 0 \\ 0 & 0 & 14.37(4) \end{pmatrix}$$

in the frame $\{X, Y, [001])\}$, where X, Y are one of $([110], [1\bar{1}0])$. The two site orientations correspond to different choices for X, Y.

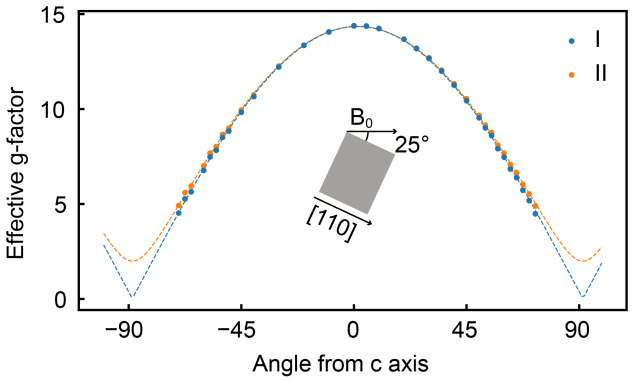

Figure S1: Angular variation of the effective g-factor of Er^{3+} when the TiO_2 is rotated about an axis 25° from [110] toward $[1\bar{1}0]$ in the ab-plane. When the sample is oriented this way, the spectrum is composed of two lines (I and II) corresponding to the two Er orientations related by a 90° rotation around the c-axis. Fitting the two series separately allows both of the weak g-factor components to be determined.

2 Experimental Details

Rutile TiO_2 samples were obtained from MTI (TOb101005S1) and implanted with doubly-ionized erbium (Innovion). The implantation was performed in multiple steps (Table S1 and Figure S2) to give a uniform density of implanted ions over a 100 nm depth, as calculated by Stopping-Range of Ions in Matter (SRIM) simulations [1].

Optical measurements were performed using an external cavity diode laser (Toptica CTL 1500) and erbium-doped fiber amplifier (PriTel). In PL and PLE experiments, the signal was detected by a high-gain InGaAs photodiode (Femto OE-200); mechanical chopping (Thorlabs MC2000B) of both the excitation and detection arms was essential to minimize scattered excitation light at the detector. For the optical-ESR measurements the excitation light was delivered via a multimode optical fiber. The sample and the fiber were both fixed to a piece of sapphire with GE varnish to maintain consistent illumination.

Implantation Energy / keV	Fluence (Low Dose) / cm^{-2}	Fluence (High Dose) / cm^{-2}
10	3.8×10^{10}	3.8×10^{12}
25	5.0×10^{10}	5.0×10^{12}
50	7.5×10^{10}	7.5×10^{12}
100	1.0×10^{11}	1.0×10^{13}
150	1.3×10^{11}	1.3×10^{13}
250	1.3×10^{11}	1.3×10^{13}
350	3.8×10^{11}	3.8×10^{13}
Total	9.0×10^{11}	9.0×10^{13}

Table S1: Implantation recipe for high and low dose sample

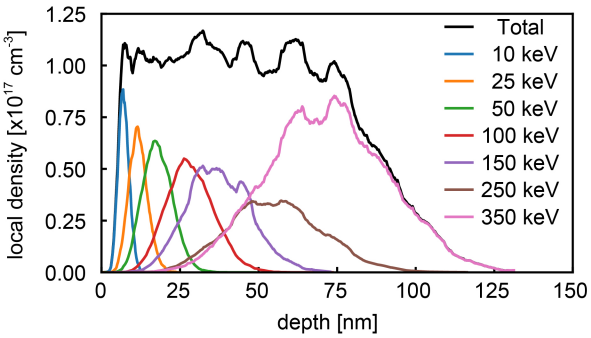

Figure S2: Simulated depth profile for each implantation step for the low dose sample. The total density profile resulting from all the steps is approximately flat down to 100 nm.

3 Annealing conditions

The samples were annealed in air in a tube furnace (Lindberg/Blue M). The annealing temperature was reached by ramping the temperature at a rate of $\approx 5°C$/min, after which the temperature was kept constant for a duration of 1h or 2h (see Table 2 in the main text), before cooling down to room temperature. This annealing process resulted in no change in the color and transparency of the samples, while annealing at the same temperatures in vacuum darkened the sample, consistent with literature reports of Ti^{4+} reduction from the creation of oxygen vacancies [2]

4 Implantation yield measurement

We estimate the number of Er^{3+} spins on the Ti^{4+} site using quantitative ESR measurements. We compare the ESR response of Er^{3+}:TiO_2 with a control sample of Er^{3+}:YSO (10 ppm, single crystal). By measuring the control and test samples simultaneously, we ensure that the temperature, cavity quality factor, and microwave power are the same. For all measurements, we also checked that the ESR spectra were taken in the linear regime with respect to microwave power and that the lines were not broadened by the magnetic field modulation. This allows us to quantitatively relate the ESR signal to the number of spins [3].

The two samples are fixed to two different pieces of single-crystal quartz held in place by a piece of cotton (Figure S3a)). We verified that the quartz and cotton pieces do not induce any perturbation signal at the magnetic fields used

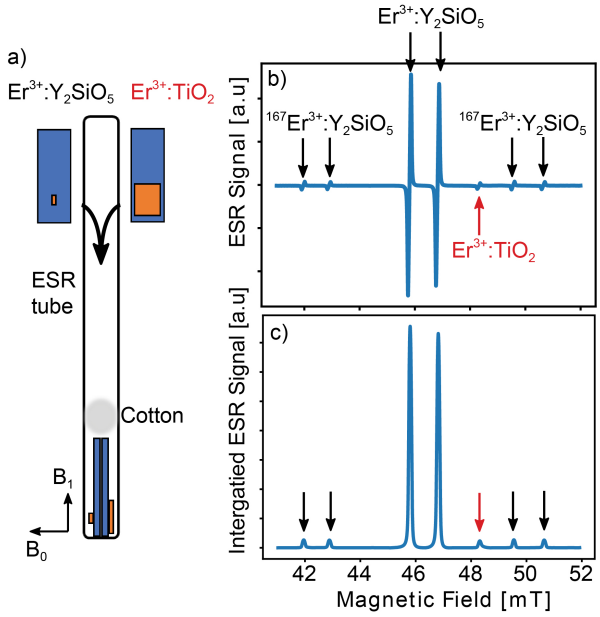

Figure S3: a) Sample arrangement in the ESR tube. b) ESR spectrum at 8 K with both the test and control samples in the cavity. Lines corresponding to Er^{3+}:YSO and Er^{3+}:TiO_2 are labeled. The magnetic field is oriented along the c-axis of the TiO_2 sample. c) Integrated spectrum corresponding to the ESR spectrum displayed in b).

for the measurements. The temperature was maintained at 8 K, which ensures that >99.9% of the Er^{3+} population is in the lowest crystal field level, so thermal occupancy to the Z_2 level is ignored.

The control sample and the orientation of the samples in the spectrometer was the same for all measurements. The samples are oriented so that $\mathbf{B_0}$ points along the c-axis of the TiO_2 sample and close to D_1 axis of the YSO sample. This orientation makes the effective g-factors of Er^{3+} ions in TiO_2 and in site 2 of YSO similar ($g_{TiO_2,||} \approx 14.4$ and $g_{YSO,||} \approx 15.1$). $\mathbf{B_0}$ is slightly misaligned (<5° in the $D_1 b$ plane) from D_1 axis of Y_2SiO_5 in order to split the two magnetically nonequivalent subsites in Y_2SiO_5 [4]. Figure S3b) shows an ESR spectrum where the signal from both samples is visible. The two strongest lines correspond to the $I = 0$ Er^{3+} isotopes in site 2 in YSO. The other four lines labeled with black arrows correspond to the $|-1/2, -1/2\rangle \leftrightarrow |1/2, -1/2\rangle$ and $|-1/2, 1/2\rangle \leftrightarrow |1/2, 1/2\rangle$ ($|m_S, m_I\rangle$ states) transitions of $^{167}Er^{3+}$ ions in the same site. The line labeled with a red arrow corresponds to the $I = 0$ Er^{3+} isotopes present in TiO_2. The oscillating magnetic field $\mathbf{B_1}$ in the cavity points along a direction close to [100] for the TiO_2 sample and close to D_2 for the YSO, for which the effective g-factors are $g_{TiO_2,\perp} = 1.41 \pm 0.31$ and $g_{YSO,\perp} = 1.86$ $(+0.8/-0.2)$ for the two samples, including the 5° misorientation.

The mass of the control sample was measured to be $m = 1.2$ mg using a 0.1 mg precision balance. The density of YSO is $d = 4.44$ g.cm^{-3}. The total concentration of Er^{3+} ions into the YSO piece is $c = 1.85 \times 10^{17}$ cm^{-3}. The number of Er^{3+} ions with $I = 0$ present in each subsite in YSO is therefore :

$$n_{YSO,I=0} = \frac{1}{2} \times \frac{1}{2} \times (1 - \eta) \times c \times \frac{m}{d} \tag{1}$$

with $\eta = 0.23$ the isotopic abundance of $^{167}Er^{3+}$. The two $\frac{1}{2}$ factors come from the fact that each site and each subsite is equally populated in YSO [5].

The double integral of the Er^{3+} peak corresponding to the $I = 0$ isotopes of the measured sample (TiO_2) was compared to both of the Er^{3+} $I = 0$ isotopes peaks of the control sample (YSO). An example of an integrated spectrum shown on Figure S3c). The area of the $I = 0$ peaks of the YSO and TiO_2 samples are determined and respectively called $A_{YSO,I=0}$ and $A_{TiO_2,I=0}$. The number of spins in the TiO_2 samples can be calculated using the expression [6]:

$$n_{TiO_2,I=0,measured} = \frac{A_{TiO_2,I=0}}{A_{YSO,I=0}} \times (\frac{g_{YSO,\perp}}{g_{TiO_2,\perp}})^2 \times n_{YSO,I=0} \tag{2}$$

The conversion efficiency is calculated as the ratio $\frac{n_{TiO_2,I=0,measured}}{n_{TiO_2,I=0,implanted}}$.

Parameter	Value	Total error	Uncorrelated error
Mass of Y_2SiO_5	1.2 mg	0.08	0
Er^{3+} concentration in Y_2SiO_5	10 ppm	0	0
$g_{TiO_2,\perp}$	1.41	0.20	0.20
$g_{YSO,\perp}$	1.86	0.20	0
$A_{YSO,I=0}$	Variable	0.10	0.10
$A_{TiO_2,I=0}$	Variable	0.10	0.10
Er^{3+} implantation dose	Variable	0.10	0
Sample area	Variable	0.10	0.10
Conversion efficiency	Variable	0.39	0.28

Table S2: Error estimations for the different parameters taken into account for conversion efficiency. Here, total error denotes the fractional uncertainty in each parameter affecting the absolute accuracy of all the measurements, while uncorrelated error denotes the fractional uncertainty contributing to relative errors between different samples.

The number of implanted spins $n_{TiO_2,I=0,implanted}$ is estimated using the implantation dose multiplied by the surface of the sample and by the isotopic abundance $(1-\eta)$. The conversion efficiencies for the different samples are displayed in the table 2 in the main text.

The error sources in measuring conversion efficiency are listed in table S2. The same reference sample was used in all cases, so uncertainty in the mass, Er^{3+} concentration and $g_{TiO_2,\perp}$ can be neglected when considering the relative uncertainty between samples.

In all samples, the observed inhomogeneous spin linewidth was around 1.1 Gauss (22 MHz).

References

[1] Ziegler, J. F.; Ziegler, M.; Biersack, J. *Nuclear Instruments and Methods in Physics Research Section B: Beam Interactions with Materials and Atoms* **2010**, *268*, 1818–1823.

[2] Khomenko, V. M.; Langer, K.; Rager, H.; Fett, A. *Physics and Chemistry of Minerals* **1998**, *25*, 338–346.

[3] Barr, D.; Eaton, S. S.; Eaton, G. R. Workshop on Quantitative EPR. 31st Annual International EPR Symposium, Breckenridge, Colorado. 2008; pp 1–125.

[4] Sun, Y.; Böttger, T.; Thiel, C. W.; Cone, R. L. *Physical Review B* **2008**, *77*, 085124.

[5] Böttger, T.; Sun, Y.; Thiel, C. W.; Cone, R. L. *Physical Review B* **2006**, *74*, 075107.

[6] Abragam, A.; Bleaney, B. *Electron Paramagnetic Resonance of Transition Ions*; Oxford University Press, 1970.